Transversal and longitudinal mixing in compound channels

G. Besio,[1] A. Stocchino,[1] S. Angiolani,[1] and M. Brocchini[2]

Received 24 April 2012; revised 5 November 2012; accepted 6 November 2012; published 15 December 2012.

[1] An experimental campaign, based on particle image velocimetry (PIV) measurements of free-surface velocities, forms the basis for an analysis of the mixing processes which occur in a compound-channel flow. The flow mixing is characterized in terms of Lagrangian statistics (absolute dispersion and diffusivity) and of the related mean flow characteristics. Mixing properties strongly depend on the ratio r_h between the main channel flow depth (h^*_{mc}) and the floodplain depth (h^*_{fp}), and three flow classes can be identified, namely shallow, intermediate, and deep flows. In the present study the large time asymptotic behavior of the mixing characteristics is analyzed in terms of the absolute diffusivity in order to characterize typical values of longitudinal and transversal diffusivity coefficients. Various sets of experiments, which cover a wide range of the governing physical parameters, have been performed and the asymptotic values of the absolute diffusivity have been evaluated. The results are then compared with several studies of flow dispersion for both the longitudinal diffusivity coefficient and the transversal turbulent mixing coefficient. The present results highlight a stronger dependence of such coefficients with the flow-depth ratio than with the flow regime (Froude number).

Citation: Besio, G., A. Stocchino, S. Angiolani, and M. Brocchini (2012), Transversal and longitudinal mixing in compound channels, *Water Resour. Res.*, *48*, W12517, doi:10.1029/2012WR012316.

1. Introduction

[2] In riverine and watercourse management it is very important to be able to understand and, possibly, predict the transport and mixing processes of contaminants, nutrients and, eventually, fine sediments. The preservation and the defense of wildlife and environmental values in natural streams is strongly dependent on the capability of modeling and analyzing the ecological impact of accidental spills or industrial dumping. These predictions, despite the many field and laboratory observations available, cannot be performed with a high level of confidence, even if recent rapid developments in water quality modeling enable a better description and a deeper understanding of pollutant behavior. The latter is, usually, modeled by a standard advection-diffusion equation for the concentration C. Such an equation enables an adequate description of the evolution of the passive tracers once the diffusivity tensor is provided. Modeling transverse and longitudinal mixing is limited by the inaccuracy and uncertainty in the prediction of coefficients typical of the mixing processes, such as the longitudinal and transverse dispersion. In general, mixing coefficients cannot be evaluated univocally by means of mathematical modeling. Usually, it is necessary to perform either field measurements or detailed and extensive laboratory experiments in order to obtain reliable figures of mixing coefficients to be used in numerical models. Great efforts have been made, during the last decades, to improve the reliability of the estimates of longitudinal and transverse mixing coefficients in rectangular open channels [*Fischer*, 1967; *Sayre*, 1968; *Sullivan*, 1968; *Prych*, 1970] [see *Fischer et al.*, 1979, and reference therein] [*Cotton and West*, 1980; *Webel and Schatzmann*, 1984; *Holly*, 1985]. Much work has also been devoted to the mixing occurring in straight uniform channels, and, subsequently, to understand and analyze the effects of both stream longitudinal curvature and width, either due to natural causes (e.g., river meandering, bottom erosion) or anthropic interventions (e.g., canalization, groins) [*Fischer*, 1969; *Holley and Abraham*, 1973; *Yotsukura and Sayre*, 1976; *Smith*, 1983; *Rutherford*, 1994; *Kashefipour and Falconer*, 2002; *Boxall and Guymer*, 2003]. Moreover, natural rivers not only commonly exhibit an irregular planar configuration, but they also are often characterized by complex cross-stream sections composed of a deep channel and shallow floodplains. These types of channels are commonly referred to as "compound channels" and their geometry is often artificially created by river engineers to restore a natural-like cross shape. In the last decades various works have been devoted to the analysis of the mixing processes and the effects of the presence of floodplains on the mixing coefficients [*Arnold et al.*, 1989; *Wood and Liang*, 1989; *Spence et al.*, 1997; *Rowinski et al.*, 2005; *Wallis and Manson*, 2005; *Fraselle et al.*, 2008; *Zeng et al.*, 2008; *Guymer and Spence*, 2009].

[3] Mixing and transport processes of solutes in compound channels are mainly controlled and regulated by the

[1]Department of Civil, Environmental and Architectural Engineering, University of Genoa, Genoa, Italy.
[2]Department of Civil and Building Engineering and Architecture, Polytechnic University of Marche, Ancona, Italy.

Corresponding author: G. Besio, Department of Civil, Environmental and Architectural Engineering, University of Genoa, Genoa 16145, Italy. (giovanni.besio@unige.it)

0043-1397/12/2012WR012316

exchange of mass and momentum between the main channel and the lateral floodplains. The main agents controlling these phenomena are the quasi-two-dimensional (2-D) macrovortical structures, which arise at the main-channel/floodplains transition region, owing to the strong generation of vorticity at the flow-depth jump. As suggested by *Nezu et al.* [1999] and verified by *Stocchino and Brocchini* [2010], the dynamics of the flow field and, hence, of the vorticity, strongly depends on the flow characteristics in terms of the flow-depth ratio r_h, between the depth in the main channel (h^*_{mc}) and the depth in the floodplains (h^*_{fp}) as first introduced by *Shiono and Knight* [1991] and later modified by *Nezu et al.* [1999]. In a more recent contribution, *Stocchino et al.* [2011] investigated the different dispersion regimes occurring in compound channel flows and highlighting the dependence of mixing both on the depth ratio r_h and on the subcritical/supercritical character of the flow, i.e., on the Froude number (Fr).

[4] The present paper follows and extends the studies of the previous contribution by *Stocchino and Brocchini* [2010] and *Stocchino et al.* [2011]. In particular, *Stocchino and Brocchini* [2010] was dedicated to the study of the characteristics of the Eulerian turbulent flow, also in relation to the still open question: Can compound channels flows be described as free mixing layers? *Stocchino and Brocchini* [2010] demonstrated that the specific geometry of the compound channels, in particular the flow-depth jump between the main channel and the floodplains, is a source of vorticity that induces the formation of quasi-2-D macrovortices that, once generated, preserve their size while being convected downstream. At that stage, the Lagrangian properties of the flow were completely ignored. *Stocchino et al.* [2011] analyzed the latter aspect in detail, studying both the single- and multiple-particle statistics, with the aim to describe the mixing regimes associated with the different flow conditions (sub- and supercritical regimes; deep, intermediate, and shallow flows). An important outcome was the demonstration that in all cases a Brownian regime exists, even if some differences have been clearly observed between the deep and the shallow flow conditions. This is important since it allows for an estimate of the asymptotic mixing coefficients. However, this aspect was not investigated by *Stocchino et al.* [2011]. In the present contribution, which can be thought as a natural extension of *Stocchino and Brocchini* [2010] and *Stocchino et al.* [2011], the scope is the evaluation of the longitudinal and transversal mixing coefficients and their dependence on the main physical parameters (the Froude number Fr and the flow-depth ratio r_h). To this end, the experimental data set has been significantly extended covering a wider range of the controlling parameters. The present study shares with *Stocchino et al.* [2011] the method used to compute the absolute statistics. However, the absolute dispersion is here needed for the estimate of the longitudinal and transversal mixing coefficients for compound channel flows, the main aim being that of contributing to the knowledge of the parameters to be used in mixing analyses.

2. Mixing: Single-Particles Statistics

[5] Mixing processes in straight compound channels can be analyzed from a Lagrangian point of view, i.e., studying material particle (passive tracers) trajectories during the flow motion [*Provenzale*, 1999; *Boffetta et al.*, 2001]. Lagrangian statistics involve averages of particle positions, in terms of single or pairs or groups of particles (absolute and relative statistics, respectively). Trends in absolute and relative diffusivities can reveal the presence of different dispersion regimes as shown by *Stocchino et al.* [2011]. Given an Eulerian velocity field it is possible to compute the trajectories of material particles by integrating the equation

$$\frac{d\mathbf{x}^*(t^*)}{dt^*} = \mathbf{u}^*(\mathbf{x}^*, t^*), \tag{1}$$

where $\mathbf{x}^* = (x^*, y^*, z^*)$ is the position at time t^* of the given particle and $\mathbf{u}^*(\mathbf{x}^*, t^*)$ is the Eulerian velocity at point $\mathbf{x}^*$ and time t^*. Hereinafter stars denote dimensional quantities. Particle trajectories form the basis for the Lagrangian analysis of the mixing process and for the computation of absolute dispersion and diffusivity. The absolute dispersion tensor $\mathbf{A}^{*(2)}$ can be written as

$$A^{*(2)}_{ij}(t^*, t^*_0) = \frac{1}{M}\sum_{m=1}^{M}\{[x_i^{*m}(t^*) - x_i^{*m}(t^*_0)][x_j^{*m}(t^*) - x_j^{*m}(t^*_0)]\}, \tag{2}$$

where M is the number of particles, $\mathbf{x}^*(t^*)$ is the position of the mth particle at time t^*, and $\mathbf{x}^{*m}(t_0)$ is its initial position. The trace of $\mathbf{A}^{*(m)}$ gives the mean square displacement, defined as the "total absolute dispersion"

$$a^{*2} = \mathrm{Trace}\left[\mathbf{A}^{*(2)}\right] = A^{*(2)}_{xx} + A^{*(2)}_{yy} \tag{3}$$

in which $A^{*(2)}_{xx}$ is the absolute dispersion in the x direction and $A^{*(2)}_{yy}$ is the absolute dispersion in the y direction. The time derivative of the absolute dispersion is the absolute diffusivity $K^{*(1)}$,

$$K^{*(1)} = \frac{1}{2}\frac{d}{dt^*}\left[\mathrm{Trace}\left(\mathbf{A}^{*(2)}\right)\right] \tag{4}$$

which can be written as

$$K^{*(1)} = K^{*(1)}_x + K^{*(1)}_y. \tag{5}$$

Under a variety of conditions, for short times after particle deployment, the absolute dispersion increases quadratically in time and then, for larger times, typically greater than the Lagrangian integral scale T^*_L, a^{*2} increases linearly within the so-called "Brownian regime." The theoretical behavior of the absolute dispersion based on Taylor's theory is systematically observed for nonhomogeneous oceanic and atmospheric velocity fields. This suggests that the asymptotic behavior of the absolute dispersion is somehow independent from the restrictive hypothesis of homogeneity [*LaCasce*, 2008, and references therein]. Equations (3) and (4) are strictly valid when the cross dispersion terms, i.e., the nondiagonal elements of the tensors $\mathbf{A}^{*(2)}$ and $\mathbf{K}^{*(1)}$, vanish. This condition is usually attained for times larger than the

Lagrangian time scale. The latter is evaluated as the time integral of the normalized velocity autocorrelation $\mathcal{R}(\tau^*)$ over the time τ^*, as already shown by *Stocchino et al.* [2011]:

$$T_L^* = \int_0^\infty \mathcal{R}(\tau^*) d\tau^*. \tag{6}$$

[6] The absolute dispersion and the absolute diffusivity have been made dimensionless by means of the Lagrangian integral time scale (T_L^*) and the time-averaged Lagrangian kinetic energy (E_L^*). With the above scaling it is easier to distinguish among the different dispersive regimes, as discussed in detail by *Stocchino et al.* [2011]. However, the purpose of the present study is the computation of the diffusivity coefficients and possibly the comparison of the present data with previous contributions. To this end, a different scaling is preferable because it is the most commonly used in this field of research. In particular, the diffusivity coefficients can be made dimensionless choosing a typical length scale and a typical velocity scale, representative of the intensity of the turbulent flow. Here we choose the hydraulic radius R^* as the relevant length scale and the bottom shear velocity u_S^* as the velocity scale: Unless the channel can be assumed as infinitely wide, the hydraulic radius is a more correct length scale than the flow depth (more details on this can be found in section 5), hence u_S^* reads

$$u_S^* = \sqrt{g i_f R^*}, \tag{7}$$

where i_f is the bottom slope.

3. Previous Laboratory Experiments and State of the Art

[7] Calculations of pollutant concentration in water bodies (e.g., rivers, reservoirs, estuaries, and oceans) are based on the solution of the advection-diffusion equation which in its three-dimensional form reads

$$\begin{aligned}\frac{\partial C^*}{\partial t^*} + u^* \frac{\partial C^*}{\partial x^*} + v^* \frac{\partial C^*}{\partial y^*} + w^* \frac{\partial C^*}{\partial z^*} = \frac{\partial}{\partial x^*}\left(D_x^{*T} \frac{\partial C^*}{\partial x^*}\right) \\ + \frac{\partial}{\partial y^*}\left(D_y^{*T} \frac{\partial C^*}{\partial y^*}\right) + \frac{\partial}{\partial z^*}\left(D_z^{*T} \frac{\partial C^*}{\partial z^*}\right),\end{aligned} \tag{8}$$

where $\mathbf{u}^* = (u^*, v^*, w^*)$ is the Eulerian three-dimensional vector field, D_x^{*T}, D_y^{*T}, and D_z^{*T} are the turbulent diffusion coefficients [see *Taylor*, 1921]. However, in most applications a simplified version of equation (8) is employed. In particular, whenever the shallow-water approximation holds, 2-D or l-D advection-diffusion equations can be derived by integrating (8) along the vertical and the transversal direction, respectively. For depth-integrated computations, streamwise and spanwise mass fluxes can be written, on the basis of a Fickian approach, in terms of the product of the gradients of the mean concentration times the following coefficients:

$$K_x^* + \overline{D_x^{*T}} \quad \text{and} \quad K_y^* + \overline{D_y^{*T}}, \tag{9}$$

where K_x^* and K_y^*, respectively, account for the dispersion effects due to the nonuniformity of the vertical profile of the longitudinal and transversal velocity, whereas $\overline{D_x^{*T}}$ and $\overline{D_y^{*T}}$ are the vertically averaged turbulent diffusion coefficients. By further integrating along the transversal direction a l-D advection-diffusion equation is obtained, in which the longitudinal mass flux is the product between the streamwise gradient of the area-averaged concentration and the following coefficient:

$$K_L^* + \overline{K_x^*} + \overline{\overline{D_x^{*T}}}, \tag{10}$$

where $\overline{K_x^*}$ is the dispersion coefficient due to the vertical flow/concentration disuniformity, $\overline{\overline{D_x^{*T}}}$ is the area-averaged turbulent diffusion coefficient, and K_L^* accounts for the longitudinal dispersive effects.

[8] The accuracy of the solution of equation (8) and of its simplified versions strongly depends on the chosen diffusivity and dispersive coefficients. For this reason major efforts have been devoted to the estimation of such coefficients; in the following we briefly recall the most relevant results, some of which are compared with our findings.

3.1. Transverse Mixing Coefficient

[9] The value of the transverse dispersion coefficient is often assumed to be a function of the bottom shear velocity and of the mean water depth as

$$K_y^* + \overline{D_y^{*T}} = A u_S^* h^*, \tag{11}$$

where A is a factor depending on the width-to-depth ratio and on the bottom friction factor.

[10] If, on the one hand, it is possible to directly measure the turbulent diffusivity $\overline{D_y^{*T}}$ separately from the dispersive term K_y^*, by limiting the effects of secondary flows, on the other hand, whenever secondary flows play a relevant role, it is impossible to separate the two contributions.

[11] In order to evaluate $\overline{D_y^{*T}}$, *Elder* [1959] performed an experimental investigation on a uniform open-channel flow in a flume characterized by a rectangular section. In particular he measured the depth-integrated concentration distribution of a tracer and by comparison with an analytical solution he was able to estimate a constant A of about 0.17. With a similar experimental setup *Okoye* [1970] found $0.1 \leq A \leq 0.2$.

[12] However, natural river flows very often differ from those evolving in rectilinear rectangular channels. Because of this, several experiments have been performed to investigate the effects of (1) cross-section variation, (2) sidewall irregularities, and (3) channel curvature. In the present context, we restrict our attention to the results obtained for straight channels that represent the closest configuration to the one employed in the present study, disregarding any curvature effects. *Holley and Abraham* [1973] studied how transverse mixing in a straight rectangular flume of constant depth was influenced by the presence of lateral groins. The authors found that $0.16 \leq A \leq 0.4$, thus concluding that secondary flows induced by groins strongly enhance lateral mixing. In a similar set of experiments, *Lau and Krishnappan* [1977]

investigated the variation of the transverse dispersion coefficient depending on different values of the friction factor and width-to-depth ratio, obtaining values of about $0.15 \leq A \leq 0.25$. Moreover, *Webel and Schatzmann* [1984] described an experimental study, performed in a 20-m-long rectangular flume, and the dependence of the mixing coefficient on different properties of the channel flow (Reynolds number, Froude number, width-to-depth ratio, and roughness), finding $0.13 \leq A \leq 0.24$. Moreover, a residual dependence on the friction coefficient remains when the flow evolves in smooth conditions. *Rutherford* [1994] in his book collected results from many studies resulting in an extended range for the transversal mixing coefficient equal to $0.1 - 0.15 < A < 0.3 - 0.4$. More recently, *Chau* [2000] proposed data on transverse mixing in an open, rectangular channel under different flow and bottom roughness conditions and, in agreement with previous works, found $0.13 \leq A \leq 0.14$.

[13] The first attempt to analyze dispersion and diffusion processes due to composite sections, such as those of compound channels, has been made by *Arnold et al.* [1989] who evaluated mixing coefficients using either a modified version of the generalized change of moment analysis or a variational method in conjunction with a finite element dispersion model. The results suggest a mean value $A = 0.45$. *Wood and Liang* [1989] employed the measures performed for a rectangular channel by *Nokes and Wood* [1988] to compare an eigenvalue-eigenfunction solution for the dispersion of effluent in a compound-like channel with some experimental data of solute dispersion performed by *Wood and Liang* [1989] themselves. The results of the analytical model revealed that values of the lateral diffusivity for rectangular channels were not in agreement with the experimental data. The same kind of approach has been followed by *Spence et al.* [1997] and *Spence et al.* [1998] who found $A \sim 0.32$. A similar value has been obtained by an experimental campaign by *Fraselle et al.* [2008], who suggested a mean value (for the main channel and the floodplains) $A = 0.21$. *Zeng et al.* [2008], using the generalized method of moments, and on the basis of data collected in a symmetric trapezoidal compound channel found $A \sim 0.26$.

[14] All the above mentioned works do not analyze the influence on the transverse mixing coefficient due to flow characteristics such as the flow-depth ratio and the Froude number.

3.2. Longitudinal Mixing Coefficient

[15] The longitudinal dispersion coefficient K_x^* was first introduced by *Taylor* [1921] as a measure of the dispersion process described by the advection-dispersion equation. *Elder* [1959] extended Taylor's theory for the dispersion in pipe flows to an open channel of infinite width and he derived an analytical solution for the longitudinal dispersion coefficient. Elder's theory assumes (1) a logarithmic vertical profile for the longitudinal velocity and (2) that the turbulent transport coefficient of momentum and mass are identical. Eventually, *Elder* [1959] derived the following relationships:

$$K_x^* = 5.93 u_S^* h^*, \tag{12}$$

$$\overline{D_x^{*T}} \sim (2/3) D_z^{*T} = (2/3) 0.067\, u_S^* h^*, \tag{13}$$

in which h^* is the water depth averaged in the transversal direction.

[16] Once the 1-D advection-diffusion equation is derived for the longitudinal direction (i.e., averaging over the depth and width), the mixing coefficient to be determined becomes the sum of three different contributions, see equation (10), where K_L^* is the longitudinal dispersion coefficient, which arises from the average along the transversal direction of the convective terms. It is usually assumed that $K_L^* \gg \overline{K_x^*}, \overline{\overline{D_x^{*T}}}$ since it is observed that longitudinal dispersion dominates longitudinal mixing due to nonuniformity of the vertical velocity profile and other geometrical nonuniformities (dead zones, curves, nonuniform depth, etc.). Most of the estimates of K_L^* for natural streams have been of empirical nature. By qualitative means *Fischer* [1975] obtained an approximated formula for the dimensionless dispersion coefficient $K_L^*/h^* u_S^*$,

$$\frac{K_L^*}{h^* u_S^*} = 0.011 \left(\frac{U^*}{u_S^*}\right)^2 \left(\frac{B^*}{h^*}\right)^2, \tag{14}$$

where U^* is the cross-sectional mean velocity and B^* is the width of the channel. The general form of dimensionless longitudinal dispersion coefficients proposed in the literature is

$$\frac{K_L^*}{h^* u_S^*} = \alpha \left(\frac{U^*}{u_S^*}\right)^{\beta} \left(\frac{B^*}{h^*}\right)^{\gamma}, \tag{15}$$

where α, β, and γ are noninteger constants. In particular, *Seo and Cheong* [1998] analyzed previous empirical equations and derived the following values of the coefficients $\alpha = 5.915$, $\beta = 0.620$, and $\gamma = 1.428$. Finally *Deng et al.* [2001], taking into account the irregularity of natural rivers and directly integrating the Fischer's triple integral, developed the following relationship for the longitudinal dispersion coefficient:

$$\frac{K_L^*}{h^* u_S^*} = \frac{0.15}{8\epsilon_{t0}} \left(\frac{U^*}{u_S^*}\right)^2 \left(\frac{B^*}{h^*}\right)^{5/3}, \tag{16}$$

where $\epsilon_{t0} = 0.145 + (1/3520)(U^*/u_S^*)(B^*/h^*)^{1.38}$.

[17] For natural open channels, the strong nonuniformity of the velocity profile between the two banks may lead to values of $K_L^*/h^* u_S^*$ that range from 5 to 7000 [*Fischer et al.*, 1979].

4. Present Experimental Campaign

[18] The experimental apparatus used in the present study consists of a straight compound channel 20 m long, 56 cm wide with a trapezoidal cross section, composed of a central main channel ($W_{mc}^* = 20$ cm), two lateral flat floodplains ($W_{fp}^* = 18$ cm) and a transition region ($W_{tr}^* = 2.5$ cm). We use a Cartesian coordinate system in which x^* and y^* are aligned with the streamwise and spanwise direction of the flow, respectively, as illustrated in Figure 1. The flume is made of sheets of polyvinyl chloride (PVC) with a Manning roughness of 0.009 $s^1\, m^{-1/3}$. The measuring area is at a distance of 10 m downstream of the flume inlet and it is characterized by fully developed flow conditions in terms of

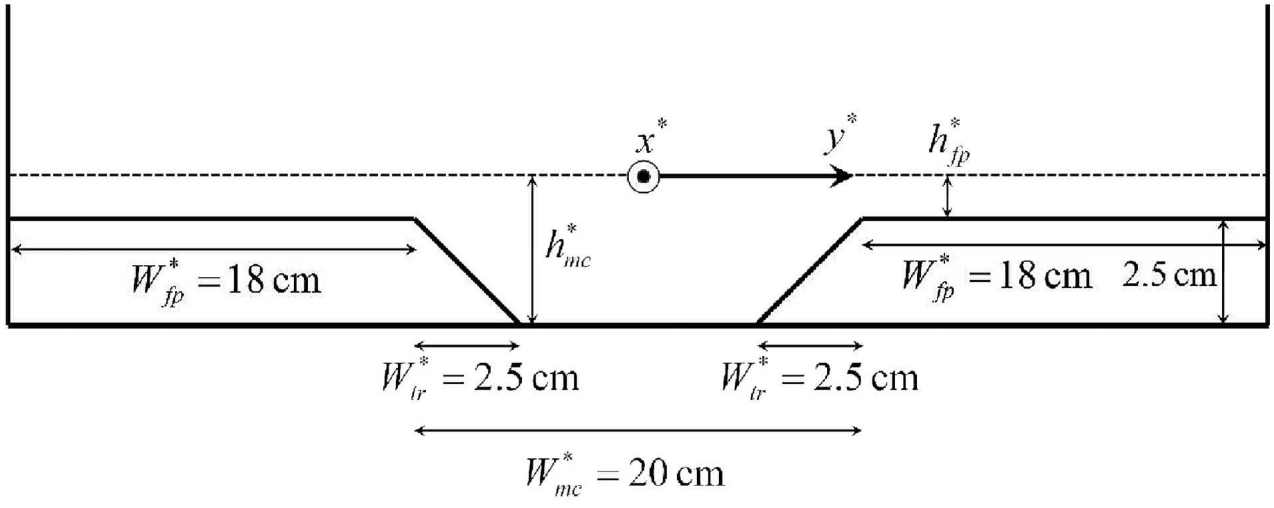

Figure 1. Sketch of the cross section of the experimental compound channel used in the present laboratory campaign.

bottom boundary layer and transition shear layer evolution [*Stocchino and Brocchini*, 2010; *Stocchino et al.*, 2011]. About 70 experiments have been performed by changing the main dimensionless experimental parameters r_h and Fr, defined as

$$r_h = \frac{h^*_{\mathrm{mc}}}{h^*_{\mathrm{fp}}}, \qquad Fr = \frac{U^*_m}{\sqrt{gR^*}}, \tag{17}$$

where h^*_{mc} is the main channel depth and h^*_{fp} is the floodplain depth, g is the gravity acceleration and U^*_m is the surface peak velocity in the main channel. The main characteristics of the experiments are grouped in Table 1 depending on the flow regimes, as suggested by *Nezu et al.* [1999], i.e., dividing shallow flows ($r_h > 3$) from the intermediate flows ($2 < r_h < 3$) and the deep flows ($r_h < 2$). In particular, in the present work several new experimental runs (series 400, 500, 800, 900) have been performed in order to investigate the behavior of the mixing processes for values of the dimensionless parameters (r_h and Fr) that were not used in the previous experimental campaigns (series 0, 00, 200, [*Stocchino et al.*, 2011]). Measurements of two-dimensional velocity fields on the free surface have been obtained by means of a 2-D PIV analysis. The PIV system consists of a high-speed digital camera (IDT xS3) with acquisition frequency between 100 and 250 Hz and an illumination system composed of four white light incandescent lamps of 500 W. Velocity measurements were made using as tracers plastic particles with a mean diameter of 150 μm. The area of interest for the flow measurements has dimensions about (1.2 × 0.6 m). The PIV technique has been used to analyze the main features of the flow under investigation and the Eulerian velocity fields are used as the basis for the computation of the tracers' trajectories and the subsequent analysis of mixing processes.

[19] For high values of the Froude number, surface waves may be generated that can possibly interfere with

Table 1. Main Experimental Parameters

Flow	Exp. Series	r_h (–)	Fr (–)	Slope (–)	Q^* (L s^{-1})	U^*_m (m s^{-1})	$Re \cdot 10^3$ (–)
Shallow	Series 00	3.05–3.69	0.63–0.73	0.0016	2.39–3.49	0.25-0.31	16.0–13.1
	Series 00	3.40–4.42	1.12–1.26	0.0048	3.55–5.25	0.42–0.52	23.9–34.9
	Series 0	3.10	1.31	0.0064	4.88–6.14	0.51–0.56	32.6–40.6
	Series 200	3.08–4.16	0.89–0.93	0.0032	2.99–4.37	0.34–0.39	20.1–28.9
	Series 400	3.15	1.64	0.0100	7.47–7.92	0.69–0.70	49.5–52.3
	Series 500	3.10–3.94	1.89–1.94	0.0140	6.68–9.07	0.73–0.82	40.5–60.0
	Series 800	3.50–4.08	1.52–1.59	0.0100	5.42–6.14	0.61–0.62	36.3–40.9
	Series 900	3.01	1.14	0.0048	5.55	0.49	36.7
Intermediate	Series 00	2.20–2.61	0.72–0.73	0.0016	4.32–5.89	0.33–0.37	28.3–37.9
	Series 00	2.36	0.92	0.0048	6.54–10.75	0.45–0.63	42.4–68.7
	Series 0	2.02–2.92	1.32–1.42	0.0064	6.68–13.54	0.57–0.75	44.0–86.1
	Series 200	2.04–2.57	0.96–1.00	0.0032	5.85–9.44	0.44–0.53	38.2–60.1
	Series 800	2.20–2.89	1.66–1.72	0.0100	8.51–13.94	0.72–0.87	56.1–89.6
	Series 900	2.23–2.65	1.17–1.20	0.0480	6.79–9.44	0.53–0.60	44.4–60.8
Deep	Series 00	1.77–1.97	0.73–0.75	0.0016	7.47–9.87	0.40–0.44	47.3–61.2
	Series 00	1.82–1.85	1.21–1.36	0.0048	14.29–16.66	0.69–0.78	89.4–103.9
	Series 0	1.85–1.96	1.43–1.45	0.0064	14.67–16.99	0.77–0.83	92.8–111.8
	Series 200	1.68–1.89	1.01–1.05	0.0032	11.31–16.07	0.56–0.64	71.1–98.2
	Series 500	1.77–1.99	2.10–2.16	0.0140	20.73–28.51	1.13–1.26	131.5–176.6
	Series 800	1.77–1.91	1.79–1.82	0.0100	19.53–24.12	0.99–1.07	122.9–149.4

the surface velocity measurements, object of the present study. In particular, roll waves are known to form for Froude numbers larger than 2. In order to avoid the generation of surface waves, we have placed at the flume inlet a polystyrene sheet, free to float on the water surface, that significantly dumps water surface oscillations of any kind.

4.1. Postprocessing of the Data

[20] In most of the experimental works discussed in section 3 the transverse mixing coefficient has been evaluated using the so-called method of moments. In particular, such a method assumes that the advection-diffusion equation for a uniform, straight-channel flow due to a continuous point-source release of contaminant has a Gaussian-type solution for the concentration. The moments of the latter distribution, e.g., the variance, are then fitted against the concentration measurements. From the time of spatial evolution of the variance the transverse dispersive coefficient is, eventually, evaluated.

[21] In the present analysis we have used a more direct approach based on the theoretical background discussed in section 2. In fact, once the 2-D Eulerian velocity fields have been obtained, an ensemble of particle trajectories has been computed by integrating equation (1), starting from a uniform seeding over the whole flow domain. We have calculated particle trajectories using a fourth-order Runge-Kutta algorithm with adaptive step size, which has a local accuracy of order $(\Delta t)^4$, where Δt is the integration time step. In more detail, for each flow field, we have seeded the experimental flow with approximately $O(5 \times 10^3)$ numerical particles (massless) on a regular grid (of constant size Δx and Δy) and, subsequently, evaluated the tracers trajectories by integrating (1) in time with the above Runge-Kutta algorithm employing a bicubic spatial interpolation and a polynomial time interpolation of the experimental Eulerian fields. From the ensemble of particle trajectories the single particle statistics, dispersion, and diffusivity have been evaluated [*Stocchino and Brocchini*, 2010; *Stocchino et al.*, 2011].

[22] The evaluation of the single-particle statistics has been performed after removal of a mean velocity profile from the Eulerian fields. In particular, the ensemble-averaged velocity along the y direction vanishes $[\overline{V}^*(x^*, y^*) = 0]$, while along the x direction the ensemble-averaged velocity $\overline{U}^*(x^*, y^*)$ assumes a bell-like profile, with the maximum located in the main channel and a velocity gradient at the transition between the main channel and the floodplains [*Stocchino and Brocchini*, 2010] which is stronger for shallower flows. For each Eulerian velocity field the mean velocity $\overline{U}^*(x^*, y^*)$, varying along the longitudinal and the transversal direction, has been subtracted from the instantaneous longitudinal velocity $u^*(x^*, y^*, t^*)$. Based on the discussion of section 3 and operating the mentioned mean flow removal, we are able to evaluate an equivalent transversal mixing coefficient which takes into account the effects of the turbulent diffusion and dispersion, as usually reported in the literature [see, e.g., *Rutherford*, 1994, and references therein]

$$K_y^{*(1)} \equiv K_y^* + \overline{D_y^{*T}} = (\text{from equation } (11)) = A u_S^* h^*. \quad (18)$$

[23] Two major mechanisms generally influence the longitudinal dispersion: (1) turbulent velocity fluctuations and (2) lateral and vertical variation of the velocity in the cross section. Because of the experimental approach (PIV measures of surface velocity) and because of the mentioned mean flow removal from the Eulerian velocity fields, we are able to provide an estimate of the turbulent diffusion term $\overline{D_x^{*T}}$ only, which is usually much smaller than the dispersion coefficient K_L^*. Hence, in the present study, the longitudinal absolute diffusivity evaluated by means of equation (4) corresponds to the turbulent diffusion

$$K_x^{*(1)} \equiv \overline{D_x^{*T}}. \quad (19)$$

[24] The approach used to numerically calculate the particle trajectories starting from measured Eulerian fields is that commonly adopted in studies of mixing [*LaCasce*, 2008]. Moreover, as already discussed by *Stocchino et al.* [2011], the computation of the particle trajectories and, therefore, of the absolute dispersion, suffers from small-amplitude, high-frequency oscillations that ultimately generate a noisy time distribution of the absolute diffusivities, which is the time derivative of a^{*2}. In the present context, where the aim is to quantify the values of the diffusivity coefficients and their dependence on the main physical parameter, it has become crucial to eliminate the spurious oscillations before computing $K_x^{*(1)}$ and $K_y^{*(1)}$. In particular, we have tested two methods. With the first approach we have filtered the absolute dispersion distribution and then we have computed the time derivative of the filtered signal and the diffusivity coefficient is eventually evaluated where its value is constant (i.e., for longer times). We have used two different filters in our procedure. In particular, the Savitzky-Golay filter, which is a generalized moving average with filter coefficients determined by an unweighted linear least-squares regression and a polynomial model of specified degree. The other filter is a local regression based on weighted linear least squares and a second degree polynomial model, where lower weight is assigned to outliers in the regression. The method assigns zero weight to data outside six mean absolute deviations. Alternatively, we have sought for the best linear regression of the filtered data, using a least-square method, of the absolute dispersion in a time range where this is meaningful, i.e., where a Brownian regime is expected.

[25] The resulting linear coefficient is directly a measure of the diffusivity coefficients. The coefficients computed with both methods resulted to be very similar, however, after several tests, the second approach proved to be more robust and it was used to produce the results that we discuss in the following.

5. Results

[26] Results obtained for single-particle statistics (absolute dispersion and absolute diffusivities) are reported as functions of time in Figures 2 and 3, for shallow and deep flow conditions, respectively. For the sake of brevity, being the proposed behavior robust over the whole set of runs, here we focus on just two sample tests. As reported by *Stocchino et al.* [2011], the dimensionless absolute dispersion a^2 displays, for both shallow and deep flow conditions, an initial ballistic regime with a quadratic growth in time (a^2 proportional to the dimensionless time t^2 where $t = t^*/T_L^*$).

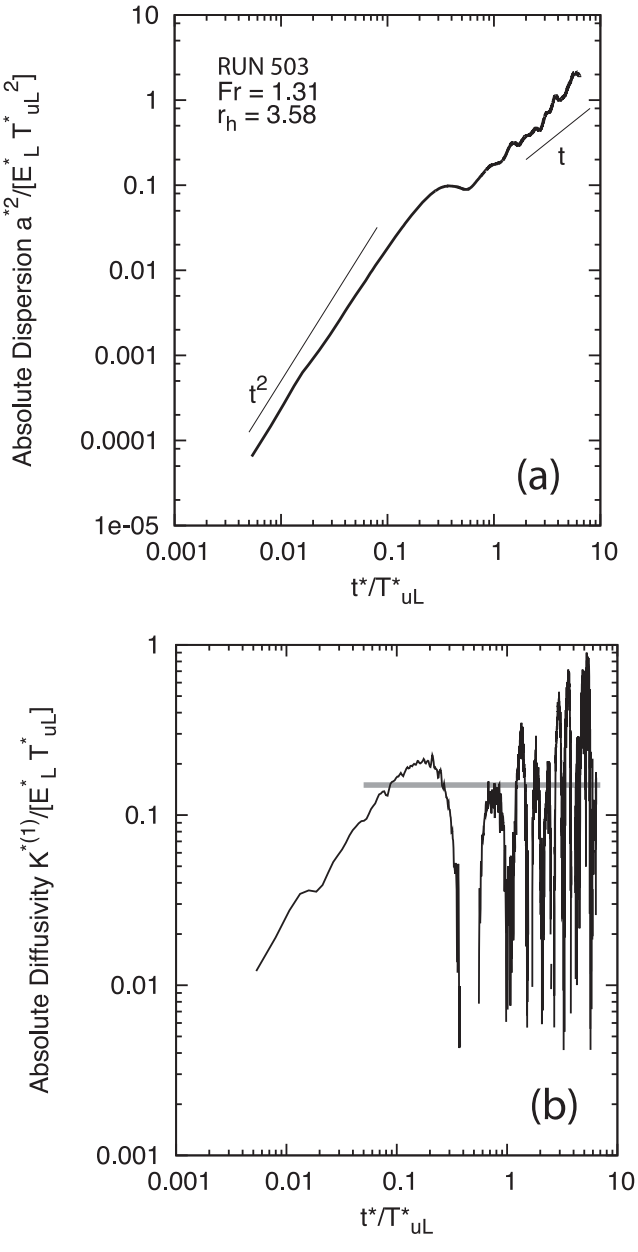

Figure 2. Single-particle statistics for experiment 503, shallow-flow conditions: (a) Absolute dispersion and (b) absolute diffusivity.

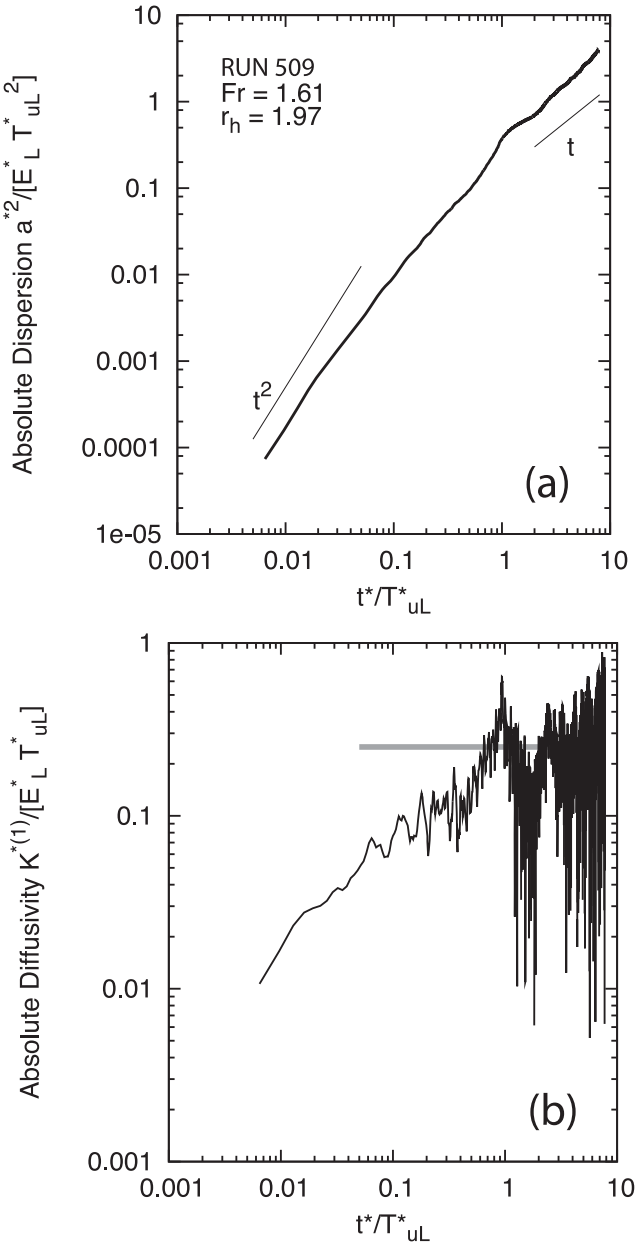

Figure 3. Single-particle statistics for experiment 509, deep-flow conditions: (a) Absolute dispersion and (b) absolute diffusivity.

[27] After the initial stage of growth, the behavior of a^2 is different for shallow and deep flow conditions. In the former case ($r_h > 3$), after a period of time almost equal to the Lagrangian time, we can observe local maxima of a^2 at times comparable with the typical time scale of the macrovortices and can be related to particle trapping in coherent vortical structures. For longer times, the absolute dispersion increases following a power of about 5/4 and, finally, it reaches the Brownian regime. On the contrary, for deep flows ($r_h < 2$), the growth of the absolute dispersion is mainly monotonic, leading to a more regular transition from the initial ballistic regime to the Brownian regime [*Stocchino et al.*, 2011].

[28] Once the asymptotic trend of the absolute dispersion is reached, the corresponding absolute diffusivity $K^{(1)}$ can be obtained by directly differentiating in time $a^2(t)$ and, not surprisingly, this shows a rather irregular time dependence, with large fluctuations caused by the high-frequency oscillation discussed in the section 4. In Figures 2 and 3 the gray horizontal lines represent the linear regressions for filtered data obtained for times larger than T^*_L. Such a behavior has been observed for the whole set of experiments.

[29] A summary of the results obtained for the asymptotic values of the dimensionless absolute diffusivity coefficients for large times is reported in Table 2. All quantities have been made dimensionless using the hydraulic radius R^* and the bottom shear velocity u^*_S of the uniform flow: Though these parameters may vary in a nonmonotone way with the flow depth in compound channels, they represent

Table 2. Experimental Measurements of Absolute Diffusivity Coefficients

Flow	r_h (–)	Fr (–)	$K_x^{*(1)}/u_S^*R^*$	$K_y^{*(1)}/u_S^*R^*$
Shallow	3.01–4.42	0.63–1.94	0.035–0.441	0.060–0.481
Intermediate	2.02–2.92	0.72–1.72	0.013–0.473	0.021–0.341
Deep	1.68–1.97	0.73–2.16	0.014–0.094	0.020–0.230

the most suited pair of variables to produce dimensionless quantities comparable throughout all geometric and flow conditions.

[30] As stated in section 1 the main physical parameters that control the dynamics of a uniform flow in a compound channel and, consequently, the Lagrangian mixing processes, are the flow-depth ratio r_h and the Froude number Fr, which discriminates the flow regimes between sub- and supercritical. For this reason, the absolute diffusivity coefficients have been analyzed in terms of their dependence on r_h and Fr. In the following we show the results for the dimensionless absolute diffusivity components in the x and y directions, $K_x^{(1)} = K_x^{*(1)}/R^*u_S^*$ and $K_y^{(1)} = K_y^{*(1)}/R^*u_S^*$, respectively.

5.1. Transversal and Longitudinal Diffusivities

[31] Results on diffusivities are proposed to satisfy both theoretical and practical modeling purposes, i.e., those of (i) collecting information to be compared with recent theoretical studies that focus on the differences existing in mixing processes between the main channel and the floodplains, with diffusivities depending on flow regimes and transversal location, i.e., main channel and floodplains [*Manson and Wallis*, 2004] and (ii) producing synthetic data to be used in practical, simplified computations of mixing that make use of one single overall value of diffusivity for the entire flow cross section. The latter approach is still very much used once numerical simulation and evaluation for practical problems, such those faced by environmental engineering, are performed.

5.1.1. Zonal Diffusivities for Main Channel and Floodplains

[32] Results are proposed for the dependence of longitudinal and transversal zonal diffusivities on both the relative flow depth (r_h) and flow intensity (Fr). Zonal diffusivities have been computed by a region-specific analysis that consists in seeding and tracking particles either in the main channel or on the floodplains. An attempt is also made to compare these results with available literature results for the dependence of $K_x^{(1)}$ with the flow intensity [*Manson and Wallis*, 2004].

[33] Figures 4 and 5 show that the dependence of both $K_x^{(1)}$ and $K_y^{(1)}$ on r_h is robust, in the sense that both zonal diffusivities (left panels, those derived for the main channel flow and right panels those for the floodplain flows) monotonically increase with the shallowness parameter r_h and with comparable growth velocities in the main channel and floodplains for $K_x^{(1)}$ (Figure 5) and a faster growth in the floodplains of $K_y^{(1)}$ (essentially due to the shallow flows, Figure 4).

[34] This is not true when considering the dependence on the flow intensity, here described by Fr (see Figures 6 and 7). In fact, while the main-channel zonal $K_y^{(1)}$ is

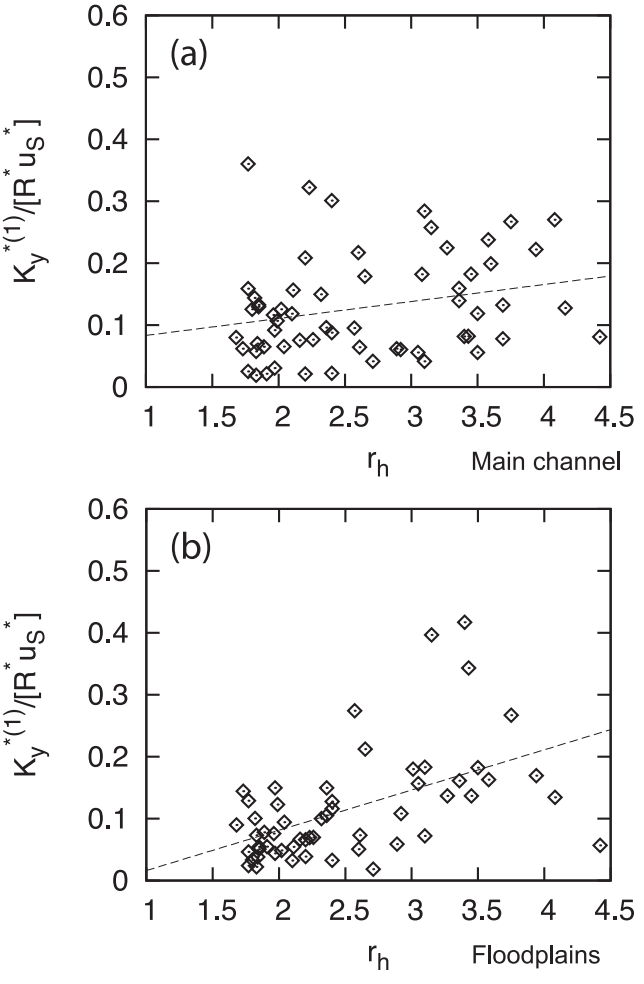

Figure 4. Dependence of the dimensionless absolute diffusivity $K_y^{*(1)}/u_S^*R^*$ on r_h for data collected in the (a) main channel and (b) floodplains. Lines indicate linear regression of the data.

directly proportional to Fr (see left panels of Figure 6), an inverse proportionality characterizes the dependence of the floodplain zonal $K_y^{(1)}$ on Fr (see right panel of Figure 6). Similarly, the floodplain zonal longitudinal diffusivity $K_x^{(1)}$ is almost independent from Fr (see the right panel of Figure 7). Although these results may be interpreted in similarity with those of *Manson and Wallis* [2004], who find an inverse proportionality of the longitudinal diffusivity with the flow rate for floods that give rise to overbank flows, care must be used because all the present results pertain to overbank flows with diffusivities computed by the mentioned zonal analysis.

[35] Zonal sowing and tracking of tracers may also give rise to problems in characterizing the role of large-scale eddies that span over the transition region, i.e., extend from the main channel to the floodplains. In this case it is virtually impossible to remove the influence of such coherent structures on the zonal diffusivities, hence leading to uncertainties in the values of the computed diffusivities. Because of this type of problem and due to the wish of providing values of diffusivities to be used for practical modeling purposes, i.e., valid over the entire flow cross section, we

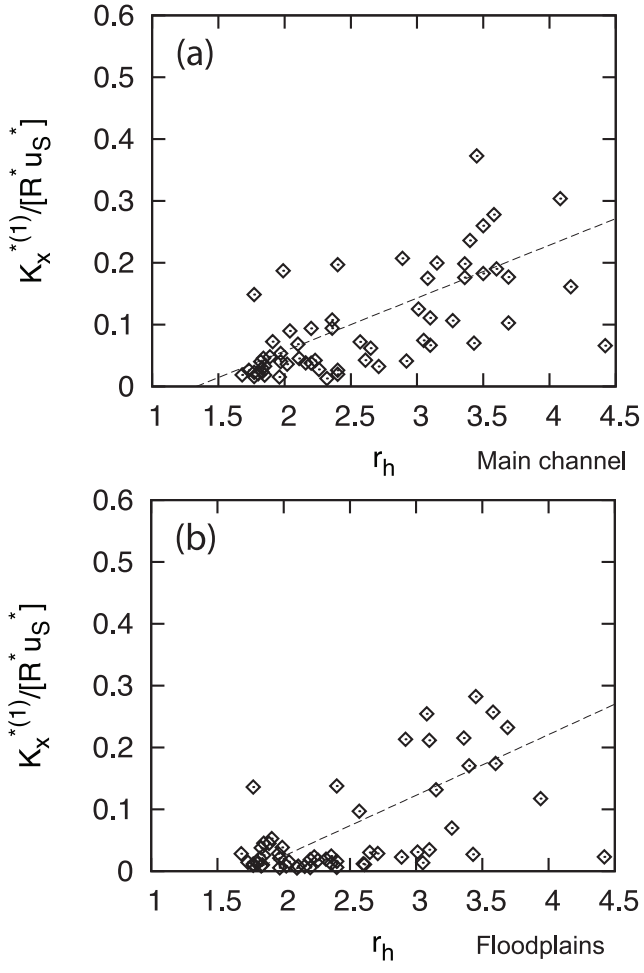

Figure 5. Dependence of the dimensionless absolute diffusivity $K_x^{*(1)}/u_S^* R^*$ on r_h for data collected in the (a) main channel and (b) floodplains. Lines indicate linear regression of the data.

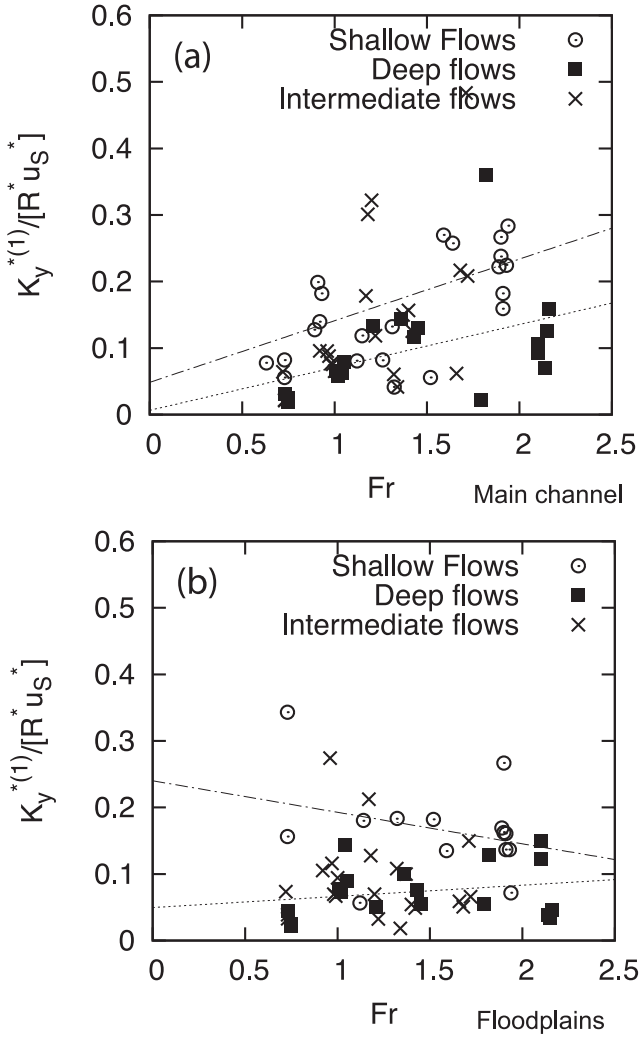

Figure 6. Dependence of the dimensionless absolute diffusivity $K_y^{*(1)}/u_S^* R^*$ on Fr for data collected in the (a) main channel and (b) floodplains. Lines indicate linear regression of the data.

focus our attention of global values of diffusivities, obtained seeding the flow over the whole compound channel cross section (i.e., main channel and floodplains).

5.1.2. Global Diffusivities for the Whole Channel

[36] Figures 8 and 9, respectively, illustrate the distributions of globally computed (i.e., over the entire cross section) diffusivities $K_x^{(1)}$ and $K_y^{(1)}$ in the $(r_h; Fr)$-parameter space. Despite a relatively large residual scatter in the estimated values, which derives from the fitting procedure described in section 4.1, the results suggest that in the $(r_h; Fr)$ plane, $K_x^{(1)}$ and $K_y^{(1)}$ increase with both the flow-depth ratio, i.e., for shallower flows, and the Froude number, i.e., for supercritical flows. The range of the experimental parameters covers a rather large interval: The Froude number spans from 0.6 to 2.2 and r_h from about 1.1 to 4.4.

[37] In Figure 10 the values of $K_y^{(1)}$ have been reported as function of the flow-depth ratio r_h and of the Froude number Fr separately, in Figures 10(a) and 10(b), respectively. The dimensionless transversal absolute diffusivity seems to monotonically increase with r_h from the deep flows toward the shallow flows, regardless of the values of the Froude number, see Figure 10(a). Despite a significant scatter of the measurements, due to the superposition of errors generated at each step (data collection, data analysis, etc.) of the complex procedure employed to estimate the mixing coefficients, an almost linear dependence on r_h can be observed. Comparably large scatter in the data is always found in similar studies [see *Rutherford*, 1994, and reference therein].

[38] The highest values of $K_y^{(1)}$ are found for the shallow-flow conditions. However, if we analyze the results as function of the Froude number Fr, see Figure 10(b), the distinction between the two limiting cases (deep and shallow flows) appears more clearly. In fact, despite an increase of $K_y^{(1)}$ with Fr, two distinct trends can be easily recognized depending on the values of r_h, revealing that shallow flows (hollow markers) lead to greater values of $K_y^{(1)}$ than deep flows (solid markers). Results for the intermediate flows nicely accommodate between the deep and shallow flow cases (cross markers).

[39] Analogous results for the streamwise coefficients $K_x^{(1)}$ are shown in Figures 11(a) and 11(b), respectively. A behavior similar to that observed for the transverse

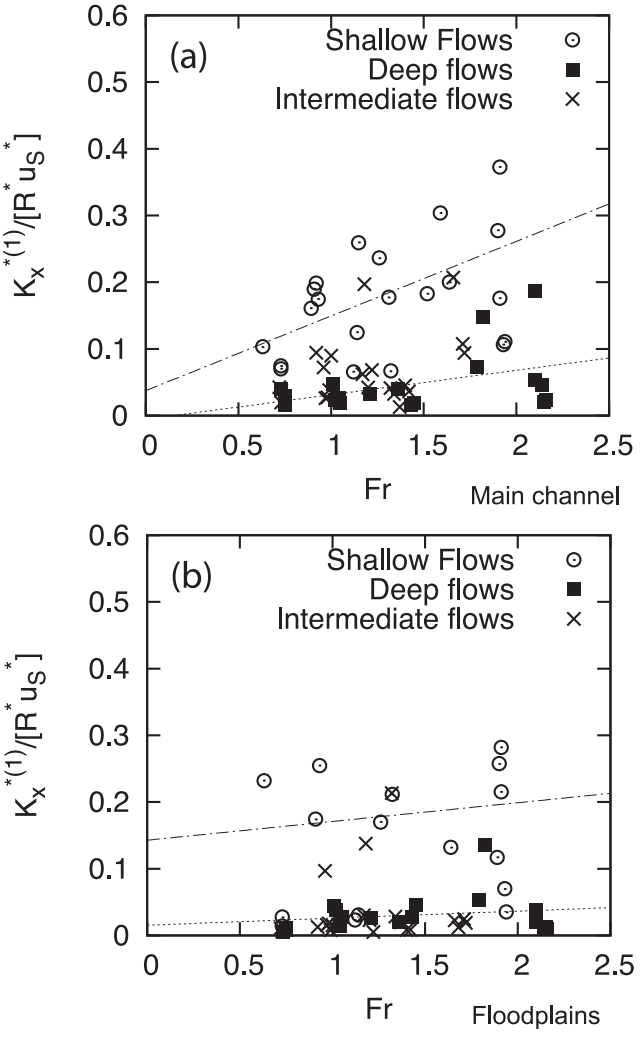

Figure 7. Dependence of the dimensionless absolute diffusivity $K_x^{*(1)}/u_S^* R^*$ on Fr for data collected in the (a) main channel and (b) floodplains. Lines indicate linear regression of the data.

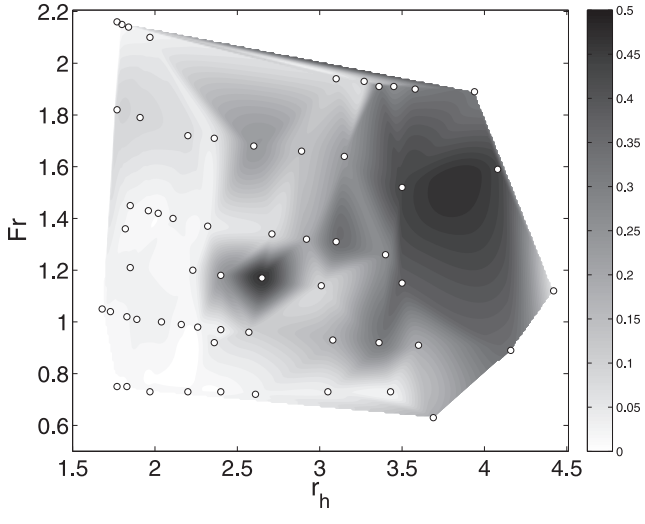

Figure 8. Distribution of the dimensionless absolute diffusivity $K_x^{*(1)}/u_S^* R^*$ in the $(r_h; Fr)$-parameter space.

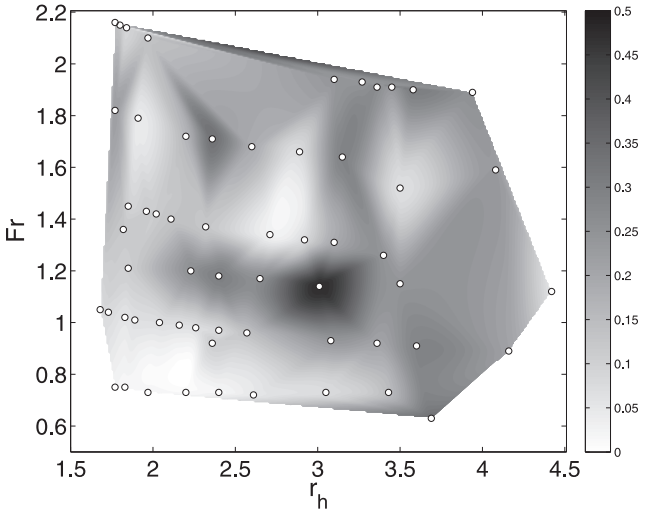

Figure 9. Distribution of the dimensionless absolute diffusivity $K_y^{*(1)}/u_S^* R^*$ in the $(r_h; Fr)$-parameter space.

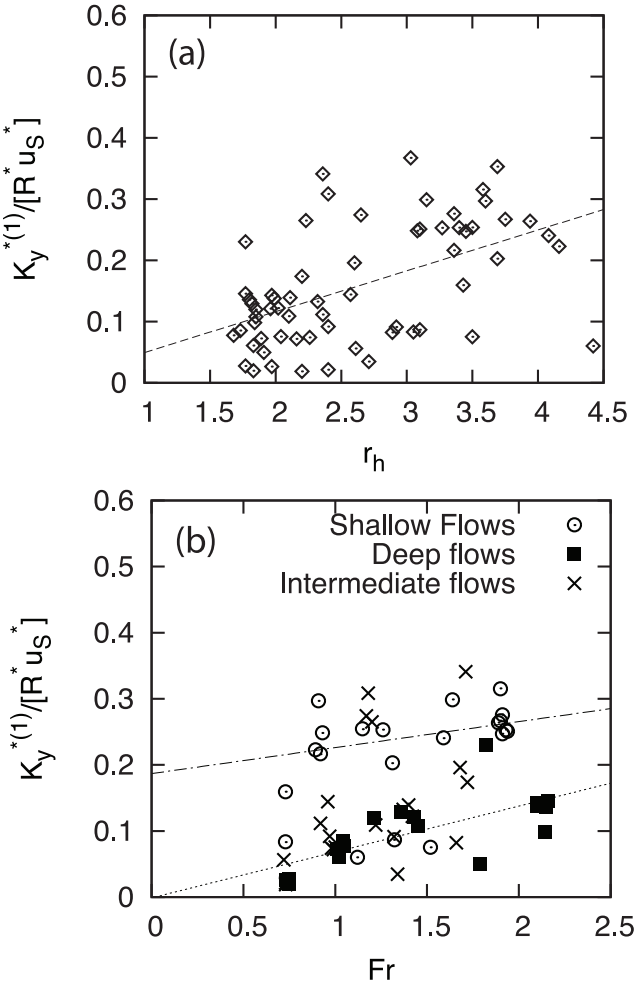

Figure 10. Dependence of the dimensionless absolute diffusivity $K_y^{*(1)}/u_S^* R^*$ on (a) r_h and (b) Fr. Lines indicate linear regression of the data.

coefficient is recovered: The longitudinal turbulent diffusivity monotonically increases with the flow-depth ratio r_h (Figure 11(a)), and shallow and deep flows are remarkably different for the same flow conditions in terms of Froude number (Figure 11(b)). Moreover, the longitudinal turbulent mixing is, not surprisingly, much less intense for the deep-flow conditions compared with the shallow cases. In fact, as described in section 4.1, $K_x^{(1)}$ only accounts for the turbulent fluctuations disregarding dispersive effects. For this reason the velocity fluctuations are less intense for the deep flows, where the two-dimensional free surface velocity fields are more uniform than for the shallow flow conditions, see *Stocchino and Brocchini* [2010] and *Stocchino et al.* [2011].

6. Discussion

[40] The main conclusions drawn in our previous similar studies [*Stocchino and Brocchini*, 2010; *Stocchino et al.*, 2011] help to explain the differences in the mixing coefficients among the all the flow conditions investigated (sub- and supercritical flows; shallow, intermediate, and deep flows).

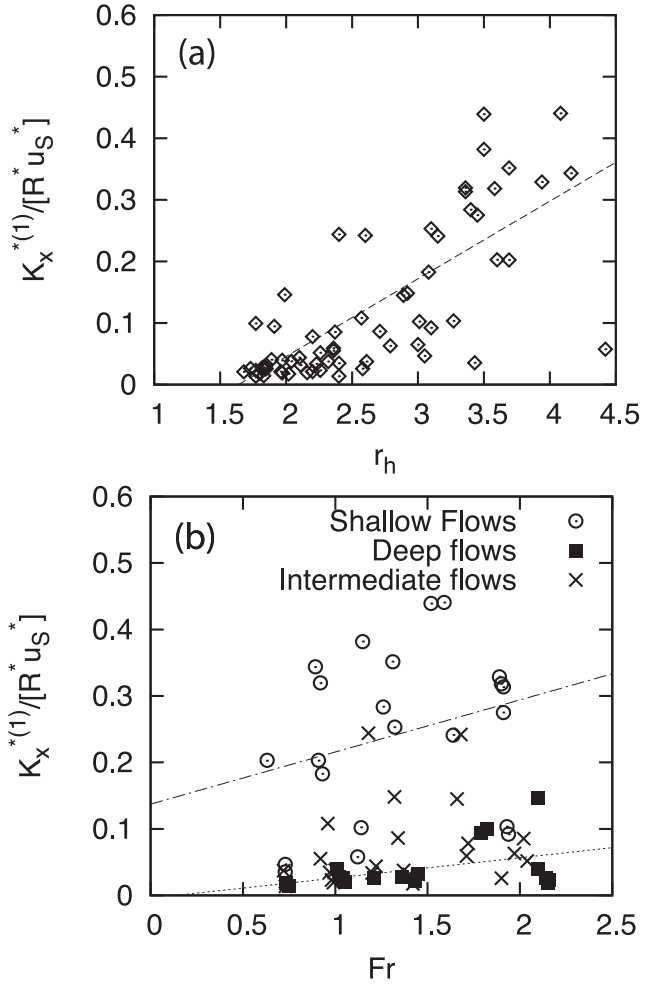

Figure 11. Dependence of the dimensionless absolute diffusivity $K_x^{*(1)}/u_S^* R^*$ on (a) r_h and (b) Fr. Lines indicate linear regression of the data.

[41] For low values of r_h (deep flows), the free-surface velocity fields are characterized by a very weak cross-flow shearing at the transition regions; there almost no two-dimensional coherent macrovortices are observed, leaving only a low content of boundary vortices, caused by the shearing at the flume sidewalls [*Stocchino and Brocchini*, 2010]. In this case, the topographic forcing at the transition region is not effective in injecting a sufficient vorticity for the generation of the macrovortices. From a Lagrangian point of view, the deep flows adapt to the classical Taylor regimes more easily than shallow and intermediate flow: A Brownian regime follows immediately after an initial ballistic regime. The energy spectra show two distinct behaviors depending on Fr: Subcritical flows are characterized by direct energy cascade while a direct enstrophy cascade characterizes supercritical flows.

[42] Both Eulerian and Lagrangian characteristics of intermediate flow are somehow closer to the ones observed for shallow flows. The surface velocity fields are dominated by both transitional vortices (as for the shallow flows) and boundary vortices (as for the deep flows), the latter ones disappearing as r_h grows, i.e., moving toward the shallow conditions. Intermediate flows are also characterized by a strong shearing at the transition region, with an intense peak of the time and x-averaged Reynolds stresses at that location [*Stocchino and Brocchini*, 2010], like the shallow flows and differently from the deep flows. An important transition occurs from an inverse energy cascade for subcritical flows to a direct enstrophy cascade for supercritical flows also. This feature is common to both intermediate and shallow flows and implies complex mechanisms, like vortex merging and elongation [*Stocchino and Brocchini*, 2010; *Stocchino et al.*, 2011]. For $Fr > 1$ the large-scale shearing dominates over the previous mechanisms leading to a change in the energy transfer. The shallow-flow transitional macrovortices are elongated vorticity patches almost aligned with the mean flow (the major axis having, on average, an angle of about 30° with the streamwise direction), which in the case of intermediate flows lose their preferential orientation [*Stocchino and Brocchini*, 2010].

[43] In the present analysis we have consistently observed that both the longitudinal and the transversal mixing coefficients increase with the flow-depth ratio. This can be explained, on the basis of the aforementioned flow characteristics, with the increase of the macrovortices content as the flow becomes shallower, see Figures 10 and 11. The action of the macrovortices, that in some cases also are modified by merging processes, results in an increase of the mass transport coefficients in both directions. Moreover, the longitudinal coefficient $K_x^{(1)}$ displays a more pronounced difference from deep to shallow flows (see Figure 11). In this case, the regularity of the free-surface velocity fields, which leads to flatter spanwise profiles of the mean streamwise velocity [see Figure 2 of *Stocchino and Brocchini*, 2010], results in a low intensity of the turbulent fluctuations and, thus, in a smaller $K_x^{(1)}$.

[44] More information can be gained by plotting the ratio between the longitudinal and transversal coefficients ($K_x^{(1)}/K_y^{(1)}$) as function of r_h (see Figure 12). The shaded area indicates the region of intermediate flows. The figure shows that deep flows, regardless the sub- or supercritical

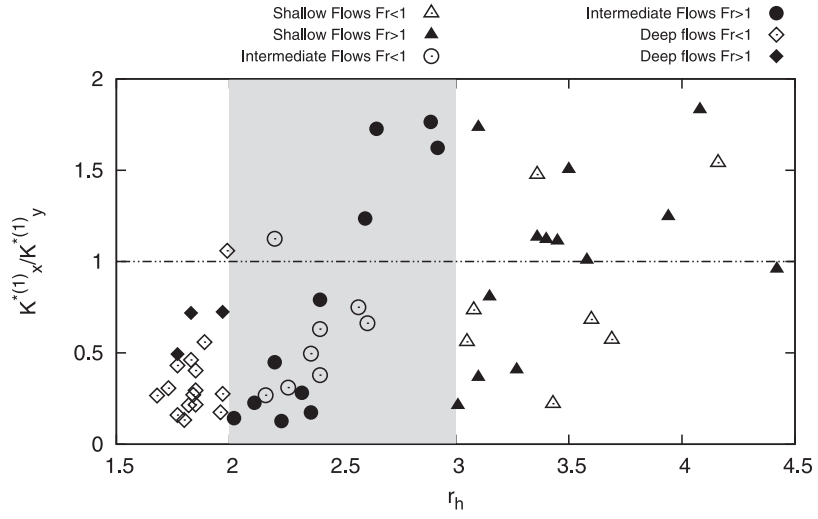

Figure 12. Dependence of the ratio $K_x^{*(1)}/K_y^{*(1)}$ on the flow-depth ratio r_h. Gray shaded zone indicates intermediate flow conditions.

regime, are characterized by a longitudinal turbulent diffusion always smaller than its transversal counterpart. On increasing r_h we find the range of intermediate flows ($2 < r_h < 2.5$) in which $K_x^{(1)}/K_y^{(1)}$ displays a behavior similar to that characterizing the deep flows. However, moving toward shallower conditions ($2.5 < r_h < 3$) a different behavior, depending on the Froude number, is observed. In fact, subcritical flows statistically lead to higher transversal coefficients, whereas for $Fr > 1$ the opposite occurs, i.e., $K_x^{(1)}/K_y^{(1)} > 1$. The latter trend is also found for shallow flows ($r_h > 3$). The dominance of the longitudinal coefficient for the supercritical flows can be ascribed to the shearing of the anisotropic mean flow that having streamwise size/intensity larger than the cross-flow ones dominates over the processes occurring at scales comparable to the macrovortex size (i.e., cross-flow size of the mean flow). In fact, as we have discussed above, the turbulent energy balance of supercritical flows is characterized by a direct enstrophy cascade, rather than an inverse energy cascade typical of the subcritical flows [*Stocchino et al.*, 2011].

[45] The present measurements can also be compared with previous experimental campaigns, already described in section 3. In Figures 13 and 14 the present results for $K_x^{(1)}$ and $K_y^{(1)}$ are directly compared with several data from previous experimental campaigns.

[46] Regarding $K_x^{(1)}$, as explained in the section 5, in the streamwise direction we are able to measure only the contribution due to turbulent diffusion. In Figure 13 only the data of *Miller and Richardson* [1974] are reported together with the theoretical prediction by *Elder* [1959]. Unfortunately, experimental data on the longitudinal turbulent diffusion are quite rare: As far as the authors are aware the data of *Miller and Richardson* [1974] are the only ones available. Even if the present experiments have been performed with a different geometrical configuration (composite section rather than rectangular cross section) and with a different roughness, much smoother than by *Miller and Richardson* [1974], the order of magnitude of the present measurements of $K_x^{(1)}$ compares well with that of the measurements by *Miller and Richardson* [1974], but surprisingly only for the shallow-flow cases. We expected the contrary to occur since a rectangular flume cannot generate macrovortices like in the case of shallow flows in a compound channel. A possible reason for the high values proposed by *Miller and Richardson* [1974] can be found in the roughness employed for the experiments, which may generate three-dimensional structures strongly affecting turbulent diffusion. The theoretical values predicted by *Elder* [1959] fall in between the values of shallow and deep flows, being anyway closer to the latter flow conditions.

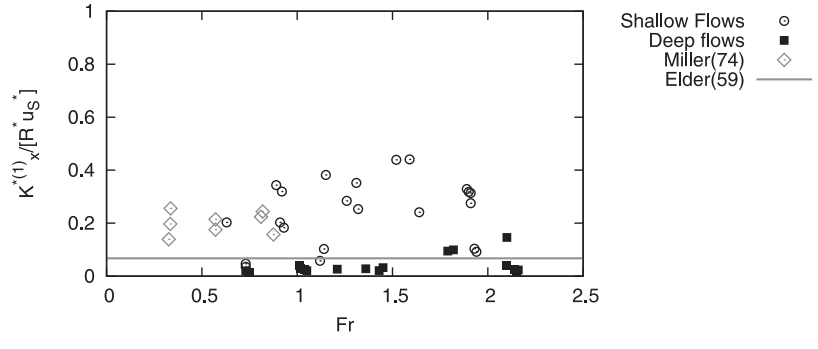

Figure 13. Dependence of $K_x^{*(1)}/u_S^* R^*$ on Fr, compared with available literature results.

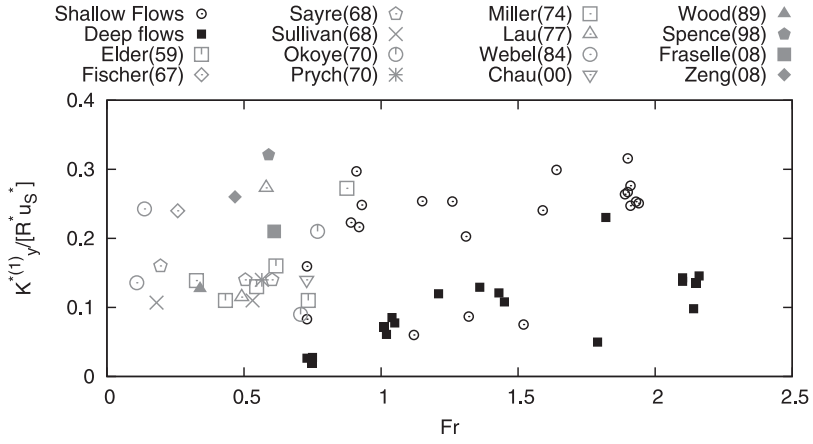

Figure 14. Dependence of $K_y^{*(1)}/u_S^* R^*$ on Fr, compared with available literature results. Gray markers: previous works (empty for rectangular channel, fill for compound channels). Black markers: present campaign.

[47] The results on the dependence of $K_y^{(1)}$ from Fr can be compared with various experimental results presented by several authors. Despite a noticeable scatter, all the literature values of $K_y^{(1)}$ coming from experiments made in rectangular flumes tend to be closer to the deep-flow cases of the present campaign. The higher values measured in rectangular-flume experiments might be due to the dependence on other flow conditions, in fact, even in previous experimental campaign it is possible to notice a quite large scatter in the outcomes for $K_y^{(1)}$ coefficient. The most evident influence on the results is due to the effect of the roughness present in the channel. For example, data obtained by *Webel and Schatzmann* [1984] and *Lau and Krishnappan* [1977] are pretty different from each other even if the value of the Froude number is almost the same. We should stress the fact that the present experimental campaign has been performed with a constant roughness, and the employment of different values of the latter could trigger different results as suggested by the range of the results obtained in previous laboratory experiments. Other differences in the magnitude of the transversal mixing coefficient for previous campaign are due to different flow conditions in terms of velocities, hence of Froude number [a.o. *Miller and Richardson*, 1974], showing an increase in $K_y^{(1)}$ with Fr, as pointed out in the present analysis. It is interesting to note that the few experiments concerning compound channel flows [*Wood and Liang*, 1989; *Spence et al.*, 1998; *Fraselle et al.*, 2008; *Zeng et al.*, 2008] show a behavior fairly similar to that observed in the present measurements. In fact, values of $K_y^{(1)}$ are smaller for deep flows [*Wood and Liang*, 1989; *Fraselle et al.*, 2008] compared with shallow flows [*Spence et al.*, 1998; *Zeng et al.*, 2008], in qualitative agreement with our observations, though the values of $K_y^{(1)}$ that we find span over a wider range of the parameters than in the literature.

[48] Finally, the values of the dispersion/diffusion coefficients, fundamental for many applications in water quality management, are consistent with the findings of *Stocchino et al.* [2011]. We confirm that these coefficients are mainly controlled by two physical parameters, namely the flow-depth ratio and the Froude number. Based on the present measurements we have derived regressions for $K_x^{(1)}$ and $K_y^{(1)}$ in the $(r_h; Fr)$-parameter space, that read

$$\frac{K_x^{*(1)}}{R^* u_S^*} = -0.129 - 0.065Fr + 0.067 r_h + 0.047 Fr\, r_h, \qquad R^2 = 0.648, \quad \mathrm{err_{var}} = 0.0060, \tag{20}$$

$$\frac{K_y^{*(1)}}{R^* u_S^*} = -0.188 + 0.131Fr + 0.094 r_h - 0.023 Fr\, r_h, \qquad R^2 = 0.386, \quad \mathrm{err_{var}} = 0.0057, \tag{21}$$

where R^2 is the coefficient of determination of the regression and $\mathrm{err_{var}}$ is an estimate of the error variance. Notwithstanding the slightly low values of the R^2, especially for $K_y^{*(1)}/R^* u_S^*$, which suggest a fairly variability in the data, relationships (20) and (21) can be easily implemented in 2-D numerical models, taking into account the variations of flow-depth ratio between the main channel and the floodplains and the overall flow regime.

7. Conclusions

[49] We have performed an extensive laboratory campaign dedicated to the evaluation of the mixing coefficients for uniform flows evolving in open compound channels. The role of the main physical parameters, namely the dimensionless flow-depth ratio r_h and the Froude number Fr, has been investigated. The experiments covered a wide range of values for both r_h and Fr, extending for the latter the range commonly studied in previous works. The present results complete the analysis discussed by *Stocchino et al.* [2011], where a detailed description of the dispersion regimes was presented, showing that deep and shallow flows evolve following different temporal laws for both the absolute and relative statistics. Moreover, different energy transfer mechanisms have also been observed for the three classes of flows. In particular, absolute statistics reveal that transitional macrovortices, typical of shallow-flow conditions,

strongly influence the growth in time of the total absolute dispersion, after the initial ballistic regime, leading to a nonmonotonic behavior. In deep-flow conditions, on the contrary, the absolute dispersion displays a monotonic growth because the generation of transitional macrovortices does not take place. This seems to have a consequence on the large-time ($t^* > T_L^*$) coefficients, as shown in the present study. However, in all cases an asymptotic diffusive regime is reached.

[50] The present analysis is based on the computation of the absolute statistics (dispersion and diffusivity) starting from the measurements of the horizontally 2-D free-surface velocity fields. The diffusivity coefficients have been computed from the long-term behavior of the absolute dispersion. A separate analysis has been performed in order to investigate the role of local flow characteristics (i.e., main channel flow and floodplains flow) on the mixing coefficient. The zonal mixing analysis is based on particle trajectories computed starting from a regular seeding of part of the cross section, the main channel, and the floodplains.

[51] Results show how zonal diffusivities for both $K_x^{(1)}$ and $K_y^{(1)}$ monotonically increase with the flow-depth ratio with a faster growth in the floodplains. On the contrary, the main channel and the floodplains behave differently considering the dependence on Froude number.

[52] Regarding the global diffusivities, the results suggest that both $K_x^{(1)}$ and $K_y^{(1)}$ monotonically increase with the decrease of the flow depth, i.e., for increasing r_h. This can be associated with the generation of 2-D macrovortices that are mainly observed at the transition region, where the flow-depth jump between the main channel and the floodplains is located. The macrovortices are responsible for an increased nonuniformity of the surface Eulerian velocity field and, thus, of the Lagrangian particle trajectories, leading to higher mixing coefficients. On the contrary, in the deep-flow condition the free-surface velocity fields are more uniform, yielding lower values of the coefficients. In particular, the longitudinal turbulent diffusivity is much lower than the transversal coefficient. The anisotropy of the coefficient is, in this case, rather pronounced.

[53] Plotting the same results as function of the Froude number, displays, again, a monotonic growth of the mixing coefficients with *Fr*. However, deep and shallow flows are clearly separated and the latter ones, for the same Froude number, are always characterized by larger values of both $K_x^{(1)}$ and $K_y^{(1)}$. Intermediate flows are placed between the two limiting cases.

[54] A comparison between the present results and several previous data has been performed for the transversal mixing coefficient and, whenever possible, also for the longitudinal turbulent coefficient. Regarding $K_y^{(1)}$, most of the measurements have been obtained in flume experiments with rectangular cross sections, which should be closer to the deep-flow condition of the present analysis. Indeed, despite a considerable scatter, on average the previous data fit better with the deep flow cases. Coherently, the experiments performed with nonrectangular cross sections show a behavior similar to the one observed in the present experimental campaign. In particular for shallow flows (see *Spence et al.* [1998] and *Zeng et al.* [2008]) the previous values are very close to the present observation. Only the data of *Fraselle et al.* [2008], with r_h close to 2, have a value slightly higher than the present data.

[55] Regarding the longitudinal turbulent diffusivity $K_x^{(1)}$, the results always show values smaller than the experimental observations collected by *Miller and Richardson* [1974] and are distributed around the theoretical value derived by *Elder* [1959].

[56] Finally, regressions for the mixing coefficients $K_x^{(1)}$ and $K_y^{(1)}$ have been provided, retaining the dependence on both the flow-depth ratio and the Froude number. These relationship might be of interest for numerical simulations based on the shallow-water advection diffusion equation applied to several applications of water quality management.

[57] **Acknowledgment.** G.B. has been supported by the University of Genoa under the framework of the Research Project "Ateneo 2010".

References

Arnold, U., J. Hottges, and G. Rouv (1989), Turbulence and mixing mechanisms in compound open channel flow, in *Proc. 23rd IAHR Congress*, pp. A-133–A-140, IAHR, Ottawa, Canada.

Boffetta, G., G. Lacorata, G. Redaelli, and A. Vulpiani (2001), Detecting barriers to transport: A review of different techniques, *Physica D*, *159*, 58–70.

Boxall, J. B., and I. Guymer (2003), Analysis and prediction of transverse mixing coefficients in natural channels, *J. Hydraul. Eng.*, *129*(2), 129–139, doi:10.1061/(ASCE)0733-9429 129: 2(129):2003.

Chau, K. (2000), Transverse mixing coefficient measurements in an open rectangular channel, *Adv. Environ. Res.*, *4*(4), 287–294, doi:10.1016/S1093-0191(00)00028-9.

Cotton, A., and J. West (1980), Field measurement of transverse diffusion in unidirectional flow in a wide, straight channel, *Water Res.*, *14*(11), 1597–1604, doi:10.1016/0043-1354(80)90064-0.

Deng, Z., V. Singh, and L. Bengtsson (2001), Longitudinal dispersion coefficient in straight rivers, *J. Hydraul. Eng.*, *127*(11), 919–927, doi:10.1061/(ASCE)0733-9429(2001)127:11(919).

Elder, J. (1959), The dispersion of marked fluid in turbulent shear flow, *J. Fluid. Mech.*, *5*(04), 544–560, doi:10.1017/S0022112059000374.

Fischer, H., E. List, R. Koh, J. Imberger, and N. Brooks (1979), *Mixing in Inland and Coastal Waters*, Academic, New York.

Fischer, H. B. (1967), The mechanics of dispersion in natural streams, *J. Hydraul. Div.*, *93*, 187–216.

Fischer, H. B. (1969), The effect of bends on dispersion in streams, *Water Resour. Res.*, *5*(2), 496–506, doi:196910.1029/WR005i002p00496.

Fischer, H. B. (1975), Discussion of "simple method for predicting dispersion in streams," *J. Environ. Eng. Div.*, *101*(3), 453–455.

Fraselle, Q., T. Arnould, X. Lissoir, D. Bousmar, and Y. Zech (2008), Investigating diffusion and dispersion in compound channels using low-cost tracer, in *Proc. River Flow 2008 Int. Conf. on Fluvial Hydraulics*, pp. 529–538, Cesme, Turkey.

Guymer, I., and K. Spence (2009), Laboratory study of transverse solute mixing during over-bank flows, in *Proc. of 33rd IAHR Congress: Water Engineering for a Sustainable Environment*, IAHR, Ottawa, Canada.

Holley, E. R., and G. Abraham (1973), Field tests of transverse mixing in rivers, *J. Hydraul. Div.*, *99*(12), 2313–2331.

Holly, F. (1985), *Dispersion in Rivers and Coastal Waters—1. Physical Principles and Dispersion Equation*, Developments in hydraulic engineering, Elsevier Applied Science, Amsterdam.

Kashefipour, S. M., and R. A. Falconer (2002), Longitudinal dispersion coefficients in natural channels, *Water Res.*, *36*(6), 1596–1608, doi:10.1016/S0043-1354(01)00351-7.

LaCasce, J. (2008), Statistics from Lagrangian observations, *Progr. Oceanogr.*, *77*, 129.

Lau, Y. L., and B. G. Krishnappan (1977), Transverse dispersion in rectangular channels, *J. Hydraul. Div.*, *103*(10), 1173–1189.

Manson, J. R., and S. G. Wallis (2004), Fluvial mixing during floods, *Geophys. Res. Lett.*, *31*(14), L14502, doi:10.1029/2004GL020452.

Miller, A. C., and E. V. Richardson (1974), Diffusion and dispersion in open channel flow, *J. Hydraul. Div.*, *100*(1), 159–171.

Nezu, I., K. Onitsuka, and K. Iketani (1999) Coherent horizontal vortices in compound open channel flows, in *Hydraulic Modeling*, edited by V. P. Singh, I. W. Seo, and J. H. Sonu, pp. 17–32, Water Resources Pub., Littleton, Colo.

Nokes, R. I., and I. R. Wood (1988), Vertical and lateral turbulent dispersion: Some experimental results, *J. Fluid. Mech.*, *187*, 373–394, doi:10.1017/S0022112088000473.

Okoye, J. K. (1970) Characteristics of transverse mixing in open-channel flows, *Tech. Rep.*, California Institute of Technology, Pasadena.

Provenzale, A. (1999), Transport by coherent barotropic vortices, *Annu. Rev. Fluid Mech.*, *31*, 55–93.

Prych, E. A. (1970), Effects of density differences on lateral mixing in open channel flows, *Tech. rep.*, Rep. No. KH-R-21, California Institute of Technology, Pasadena, California.

Rowinski, P., W. Czernuszenko, and M. Krukowski (2005), *Water Quality Hazards and Dispersion of Pollutants*, pp. 121–141, Springer, Berlin.

Rutherford, J. C. (1994), *River Mixing*, Wiley, New York.

Sayre, W. W. (1968), A laboratory investigation of the open channel dispersion processes for dissolved, suspended, and floating dispersants, *U.S. Geol. Surv. Prof. Pap.*, *433-E*, E1–E71.

Seo, I. W., and T. S. Cheong (1998) Predicting longitudinal dispersion coefficient in natural streams, *J. Hydraul. Eng.*, *124*(1), 25–32, doi:10.1061/(ASCE)0733-9429 124: 1(25):1998.

Shiono, K., and D. Knight (1991), Turbulent open-channel flows with variable depth across the channel, *J. Fluid Mech.*, *222*, 617–646.

Smith, R. (1983), Longitudinal dispersion coefficients for varying channels, *J. Fluid. Mech.*, *130*, 299–314, doi:10.1017/S002211208300110X.

Spence, K., R. Potter, and I. Guymer (1997) Transverse solute mixing from river outfalls during overbank flows, in *Proc. 3rd Int. Conf. on River Flood Hydraulics*, pp. 485–494, HR Wallingford Ltd, South Africa.

Spence, K., I. Guymer, and J. R. B. Sander (1998), Transverse mixing of solute and suspended sediment from a river outfall during over-bank flow, in *Proc. of 7th Int. Symp. on River Sedimentation and 2nd Int. Symp. on Environmental Hydraulics*, pp. 363–368, Hong Kong, China.

Stocchino, A., and M. Brocchini (2010), Horizontal mixing of quasi-uniform, straight, compound channel flows, *J. Fluid. Mech.*, *643*, 425–435.

Stocchino, A., G. Besio, S. Angiolani, and M. Brocchini (2011), Lagrangian mixing in straight compound channel, *J. Fluid. Mech.*, *675*, 168–198, doi:10.1017/S0022112011000127.

Sullivan, P. J. (1968), Dispersion in a turbulent shear flow, Ph.D. thesis, University of Cambridge, Cambridge, England.

Taylor, G. (1921), Diffusion by continuous movement, *Proc. London Math. Soc.*, *20*, 196–212.

Wallis, S., and R. Manson (2005), *Water Quality Hazards and Dispersion of Pollutants*, pp. 69–84, Springer, Berlin.

Webel, G., and M. Schatzmann (1984), Transverse mixing in open channel flow, *J. Hydraul. Eng.*, *110*(4), 423, doi:10.1061/(ASCE)0733-9429 110: 4(423):1984.

Wood, I. R., and T. Liang (1989), Dispersion in an open channel with a step in the cross-section, *J. Hydraul. Res.*, *27*(5), 587–601, doi:10.1080/00221688909499112.

Yotsukura, N., and W. W. Sayre (1976), Transverse mixing in natural channels, *Water Resour. Res.*, *12*(4), 695–704, doi:197610.1029/WR012i004 p00695.

Zeng, Y., W. Huai, and I. Guymer (2008), Transverse mixing in a trapezoidal compound open channel, *J. Hydrodyn. Ser. B*, *20*(5), 645–649, doi:10.1016/S1001-6058(08)60107-9.